

# Australian Monsoon Variability Driven by a Gill–Matsuno-Type Response to Central West Pacific Warming

ANDRÉA S. TASCHETTO

*Climate Change Research Centre, University of New South Wales, Sydney, New South Wales, Australia*

REINDERT J. HAARSMA

*Royal Netherlands Meteorological Institute, De Bilt, Netherlands*

ALEXANDER SEN GUPTA, CAROLINE C. UMMENHOFER, KHALIA J. HILL, AND MATTHEW H. ENGLAND

*Climate Change Research Centre, University of New South Wales, Sydney, New South Wales, Australia*

(Manuscript received 16 October 2009, in final form 22 April 2010)

## ABSTRACT

The objective of this study is to investigate the mechanisms that cause the anomalous intensification of tropical Australian rainfall at the height of the monsoon during *El Niño Modoki* events. In such events, northwestern Australia tends to be wetter in January and February when the SST warming is displaced to the central west Pacific, the opposite response to that associated with a traditional *El Niño*. In addition, during the bounding months, that is, December and March, there is below-average rainfall induced by an anomalous Walker circulation. This behavior tends to narrow and intensify the annual rainfall cycle over northwestern Australia relative to the climatology, causing a delayed monsoonal onset and an earlier retreat over the region. Observational datasets and numerical experiments with a general circulation model are used to examine the atmospheric response to the central west Pacific SST warming. It is shown here that the increase of precipitation, particularly in February, is phased locked to the seasonal cycle when the intertropical convergence zone is displaced southward and the South Pacific convergence zone is strengthened. An interaction between the interannual SST variability associated with *El Niño Modoki* events and the evolution of the seasonal cycle intensifies deep convection in the central west Pacific, driving a Gill–Matsuno-type response to the diabatic heating. The westward-propagating disturbance associated with the Gill–Matsuno mechanism generates an anomalous cyclonic circulation over northwestern Australia, leading to convergence of moisture and increased precipitation. The Gill–Matsuno-type response overwhelms the subsidence of the anomalous Walker circulation associated with *Modoki* events over Australia during the peak of the monsoon.

## 1. Introduction

The leading two modes of sea surface temperature (SST) variability in the tropical Pacific defined by an empirical orthogonal function (EOF) analysis are characterized by a canonical *El Niño* pattern and a warming in the central Pacific extending to the date line. This central Pacific warming pattern has been called *Trans-Niño* by Trenberth and Stepaniak (2001), *date-line El Niño* by Larkin and Harrison (2005), and more recently as *El Niño*

*Modoki* by Ashok et al. (2007). Despite the slightly different definitions, they refer to essentially the same SST structure.

Ashok et al. (2007) describe the *El Niño Modoki* pattern as a warming in the central Pacific flanked by cool SST anomalies on both sides of the oceanic basin (Fig. 1a). The authors define an index, the *El Niño Modoki Index* (EMI), as the difference between the SST anomalies averaged over the central Pacific and the averaged SST anomalies of the combined eastern and western sides of the Pacific. The EMI exhibits low-frequency variability on decadal time scales with more frequent occurrences after 1979. Because of its low-frequency modulation, Luo et al. (2008) hypothesized that *Modoki* is closely related to decadal variability in the tropical Pacific, suggesting

---

*Corresponding author address:* Andréa S. Taschetto, Climate Change Research Centre, University of New South Wales, Sydney, NSW, 2052, Australia.  
E-mail: a.taschetto@unsw.edu.au

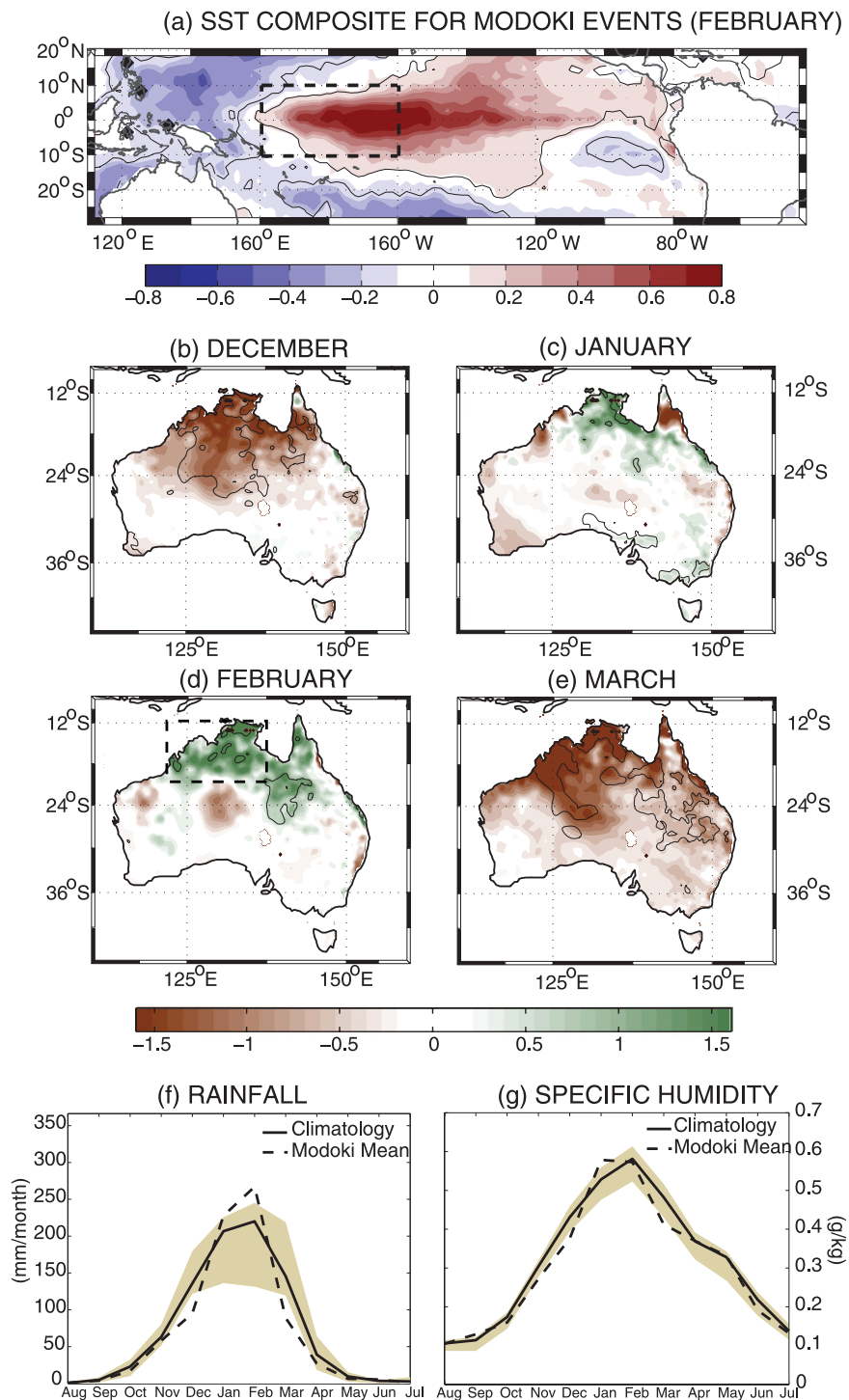


FIG. 1. Composites during Modoki years. (a) SST anomalies ( $^{\circ}\text{C}$ ) in February. Dashed box represents the region where a  $1^{\circ}\text{C}$  anomaly was superimposed onto the mean SST seasonal cycle in the sensitivity experiment. (b)–(e) Rainfall anomaly ( $\text{mm day}^{-1}$ ) from December to March. Areas within the thin black contours are significant at the 95% level based on a Student's  $t$  test. Annual cycles of (f) rainfall and (g) specific humidity at the surface for the averaged northwestern Australia region are shown in (d) (dashed box), where rainfall anomalies are largest. The solid lines are climatology and the dashed lines are the composited Modoki years. Values outside the shaded area are significant at the 90% confidence level based on a Monte Carlo test.

a greater predictability for Modoki events than interannual El Niños. The greater predictive skill of Modoki events compared to conventional El Niños has also been reported by Kim et al. (2009).

Despite growing interest, the mechanism behind a Modoki onset and its evolution are still under debate. Ashok et al. (2007) propose that Modoki events are completely independent from traditional El Niños. According to the authors, the recent weakening of equatorial easterlies in the central Pacific and enhanced easterlies to the east has decreased the zonal SST gradient and flattened the thermocline, resulting in a climate state more favorable for Modoki evolution. In contrast, Trenberth and Smith (2009) argue that the first two modes of variability in tropical Pacific SST anomalies play complementary roles in the evolution of El Niño–Southern Oscillation (ENSO) events, with the Modoki episodes leading the canonical El Niño by 4–6 months.

Regardless of the mechanisms driving El Niño Modoki events, it is clear that its impacts are distinct from those of traditional El Niños. Instead of a single anomalous Walker cell, El Niño Modoki drives two anomalous cells in the troposphere with the joint ascending branch displaced to the central equatorial Pacific (Ashok et al. 2007; Wang and Hendon 2007). The different atmospheric circulation results in a distinct regional climate response compared to traditional El Niños (Ashok et al. 2007; Trenberth and Smith 2009). Indeed, Branstator (1985) used a linear barotropic model to show that the large-scale atmospheric circulation can be very sensitive to the position of the equatorial Pacific SST forcing.

The climate impacts associated with the different flavors of El Niños have been a subject of growing research in the past few years. For instance, Weng et al. (2007) show that Modoki events tend to dry areas in the United States, China, and Japan that normally receive average to above-average rainfall during canonical El Niños. Kumar et al. (2006) suggest that Modoki episodes are more effective in causing dry conditions over India than conventional El Niños. Kim et al. (2009) show that events with maximum SST anomalies near the date line are associated with an increased frequency of North Atlantic tropical cyclones.

Over Australia, Wang and Hendon (2007) suggest that regional climate is sensitive to the location of the SST warming in the equatorial Pacific. Taschetto et al. (2009) used idealized numerical experiments to corroborate the Wang and Hendon (2007) hypothesis. By placing anomalous warming at different longitudes along the equatorial region, they show that the strongest precipitation response over Australia occurred when the SST warming is centered on the date line. Taschetto et al. (2009) also suggested that the slight cooling on both sides of the

tropical Pacific that accompanies the central warming in a Modoki signature does not significantly affect the rainfall response in Australia. Instead, they argue the positive SST anomalies around the date line are the main driver of Australian monsoon variations.

Overall, Australian rainfall is below average during Modoki events because of subsidence caused by the anomalous Walker cell. The anomalous dry conditions are particularly strong in the north for the autumn season, that is, March–May (MAM; Taschetto and England 2009). Surprisingly, correlations between Australian rainfall and the EMI in austral summer [December–February (DJF)] are weak and nonsignificant, despite the same Modoki SST signature in the tropical Pacific. In an attempt to solve this conundrum, Taschetto et al. (2009) examined the month-to-month evolution of the relationship between Australian rainfall and EMI. They found that Australia experiences wet conditions in February and below-average rainfall in December, with January as a transitional month. Thus, in the averaged DJF season, the positive rainfall anomaly in February counteracts the negative response in December, giving the false impression that Modoki does not impact Australian rainfall during austral summer.

Enhanced precipitation over Australia associated with El Niño Modoki events contradicts the present paradigm regarding the relationship between warm events in the tropical Pacific and droughts over the continent. Taschetto et al. (2009) reveal that the above-normal rainfall in February is associated with anomalous cyclonic circulation and thus a convergence of moisture over northwestern Australia. This bimodal behavior in austral summer rainfall over northern Australia has important implications for the monsoon. While there is plentiful rainfall in February, northern Australia is subjected to dry conditions in December and March during Modoki years. Thus, northern Australia experiences a shorter but more intense monsoon associated with an SST warming in the tropical Pacific around the date line compared to the climatology. The climate dynamics driving these variations in rainfall, circulation, and moisture convergence are not yet well understood.

In this study, we extend the work of Taschetto et al. (2009) to investigate the mechanisms that produce the anomalous cyclonic circulation over northwestern Australia during El Niño Modoki events. As the convergence of moisture and enhanced precipitation associated with Modoki events occurs at the peak of the Australian monsoon only, we hypothesize that this is phase locked to the seasonal variations in the mean state. We show that the anomalous warming around the date line, together with the intense convergence zone in February, leads to increased diabatic heating that drives enhanced convective

processes. Deep convection is conducive to atmospheric perturbations in a Gill–Matsuno-type mechanism that propagates a cyclonic flow to the west of the diabatic heating.

This paper is presented as follows: section 2 describes the datasets and atmospheric general circulation model (AGCM); section 3 examines the Australian monsoon; sections 4 and 5 characterize the climatological state in the tropical Pacific; section 6 describes the mechanism related to the anomalous response over Australia; and section 7 summarizes the main findings of this study.

## 2. Methodology and datasets

We analyze the climatology and anomalies for the period 1979–2006, when the introduction of satellite measurements provides more reliable temporal and spatial observations. To characterize episodes with the maximum warming located in the central tropical Pacific, we calculate composites of SST and atmospheric quantities for El Niño Modoki events. The composite of Modoki events is based on Ashok et al. (2007)'s classification, starting in June and ending in May of the subsequent year: 1979/80, 1986/87, 1990/91, 1991/92, 1992/93, 1994/95, 2002/03, and 2004/05.

### a. Observations and reanalyses

In this study, we examine monthly sea level pressure, outgoing longwave radiation (OLR), precipitation, specific humidity, diabatic heating, streamfunction, velocity potential, and horizontal winds from the National Centers for Environmental Prediction (NCEP)–National Center for Atmospheric Research (NCAR) reanalysis (Kalnay et al. 1996). The vertically integrated moisture flux and its divergence were calculated using humidity and winds from the NCEP–NCAR reanalysis.

The monthly SST dataset is the global sea ice and sea surface temperature analyses from the Hadley Centre Global Sea Ice and Sea Surface Temperature version 1 (HadISST1). The HadISST1 data have a spatial resolution of  $1^\circ$  latitude  $\times$   $1^\circ$  longitude and has been shown to be an improvement upon the Global Sea Ice and Sea Surface Temperature dataset (GISST; Rayner et al. 2003).

We use the rainfall dataset from the Australian Bureau of Meteorology (Lavery et al. 1992). The data have been constructed using various spatial interpolation algorithms to estimate rainfall across Australia on a monthly time scale. The interpolated surface is given on a regular  $0.5^\circ$  grid over the continent. To examine daily time scales, we also use the rainfall dataset from the NCEP–Department of Energy (DOE) Atmospheric Model Intercomparison Project II (AMIP-II) Reanalysis. The NCEP–DOE reanalysis 2 is an improved version of the NCEP–NCAR

reanalysis, fixing certain errors and using updated parameterizations of physical processes (Kanamitsu et al. 2002).

### b. The atmospheric model and numerical experiments

The AGCM used in this study is the NCAR Community Atmosphere Model, version 3 (CAM3). The configuration of CAM3 used here has T42 spectral truncation in the horizontal (approximately  $2.8^\circ$  latitude  $\times$   $2.8^\circ$  longitude) and 26 vertical levels in sigma–pressure hybrid coordinate. A detailed description of CAM3 can be found in Collins et al. (2004). NCAR CAM3 adopts the parameterization scheme developed by Zhang and McFarlane (1995) to represent deep convection processes. The performance of the hydrological cycle in CAM3 is detailed by Hack et al. (2006).

We conducted an idealized experiment consisting of a 50-member ensemble. Each member was integrated for 12 months and started with a slightly different initial atmospheric state to account for the internal variability in the system. The boundary forcing consisted of a monthly varying SST climatology based on long-term means from the HadISST1 dataset. Onto this, an idealized  $1^\circ\text{C}$  SST warming is superimposed in the central west equatorial Pacific, bounded between  $10^\circ\text{N}$  and  $10^\circ\text{S}$  and centered on the date line from  $160^\circ\text{E}$  to  $160^\circ\text{W}$ . The idealized SST anomalies were linearly tapered to zero over a  $10^\circ$  latitude–longitude band to reduce unrealistic atmospheric responses due to sharp gradients at the edges of the perturbation. This forcing area is a key region of the Modoki SST pattern for impacts on Australian rainfall and climate (Taschetto et al. 2009). Arblaster et al. (2002) also used similar perturbation experiments to show that Australian rainfall is more sensitive to positive SST anomalies in the west than the east tropical Pacific.

## 3. The Australian monsoon response to Modoki events

A typical Australian monsoon starts in December, peaks in January and February, and ends in March (Suppiah 1992). During the monsoon, the tropical latitudes over Australia experience changes in pressure and winds that lead to heavy rainfall over the region. However, during Modoki events, Australian rainfall tends to decrease in December and March (Figs. 1b and 1e) and become enhanced during January and February (Figs. 1c and 1d), especially over the northwest (Taschetto et al. 2009). As a consequence, the annual cycle of rainfall over northwestern Australia (averaged region  $12^\circ$ – $20^\circ\text{S}$ ,  $120^\circ$ – $135^\circ\text{E}$ ) during Modoki years is shorter and more intense compared to the climatology (Fig. 1f). The

shortening and intensification of the Australian monsoon seems to be a robust feature, appearing not only in the gridded database on station measurements [Bureau of Meteorology (BoM) data] but also in the datasets based on satellite data [i.e., Climate Prediction Center (CPC) Merged Analysis of Precipitation (CMAP)] and even in the rainfall composite from the NCEP–NCAR reanalysis that is model generated. Similarly, the annual cycle of specific humidity is consistent with that of rainfall (Fig. 1g). Specific humidity over northwestern Australia shows a significant decrease in December and March and an increase in January, while February maintains the same amount of moisture over the region.

To examine whether Modoki events can lead to a delayed monsoon onset and an earlier retreat over Australia, we use daily rainfall to calculate the start and end date of the rainy season for every year of the period 1979–2006. To estimate the large-scale onset and retreat dates of the rainy season, we have adopted a similar definition to that used by Nicholls (1984) and Smith et al. (2008). The onset of a rainy season is defined as the day when the accumulated rainfall reaches 15% of the annual total, and the end date when 85% of total rainfall is accumulated. The accumulated annual rainfall is calculated from July of the previous year to June of the next year. The result shown here is consistent with the rainy window adopted by Smith et al. (2008), from 1 September to 30 April. This simple estimate is satisfactory for our purposes, because we are not interested in the actual dates of the monsoon, but rather in the difference between the start and end of the rainy season during the composited Modoki years compared to the climatology.

Figure 2 shows the difference in the mean monsoon onset date and retreat between Modoki years and the climatology. We focus only on the regions characterized by a well-defined rainy season in austral summer, as shown in Fig. 2. This area was selected as the region where the DJF accumulated precipitation was larger than 50% of the total accumulated climatological rainfall.

Northern Australia shows an overall delay in the start of the rainy season for the composited Modoki years, as depicted by the positive contours in Fig. 2a. Conversely, the difference in the monsoon retreat between the composited Modoki years and the climatology is negative over most of northern Australia (Fig. 2b), indicating an earlier retreat of the monsoon during the Pacific warm events. The delay in the monsoon onset over the defined region varies from less than a week in the far northeast to as much as 25 days in the southwest. Averaged over the Australian region to the north of 20°S the delay is about 7.4 days, while the retreat is approximately 6.5 days, that is, about one week. If the rainy window is taken from September to April, as in Smith et al. (2008), the onset

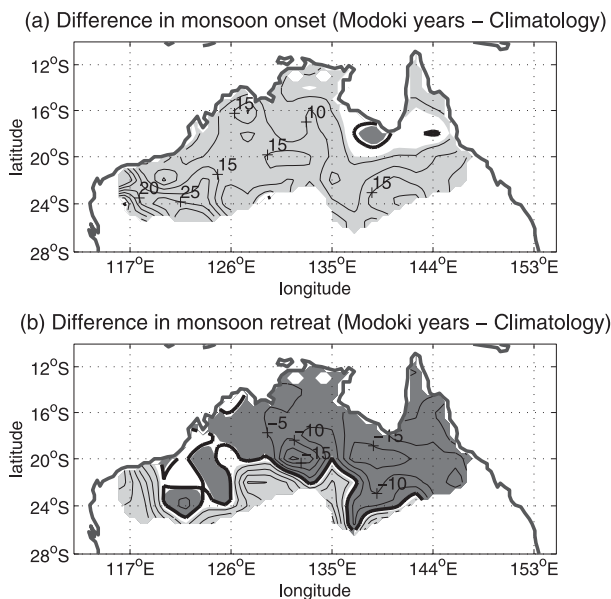


FIG. 2. The shift (days), in the (a) monsoon onset or (b) monsoon retreat between the composited Modoki years and the climatology. Light-gray (dark gray) areas indicate a delay (advance) in the onset (retreat) of the rainy season. Only regions with a rainy season in DJF are plotted here. Contour intervals are 5 days. The zero contour is represented by the black thick lines.

and retreat are both offset by just over 1 week. Although a difference of 1 week in the advance and retreat of the monsoon does not appear too large, it is sufficient to produce significant change to the normal monthly rainfall totals. A significant fraction of northern Australia, however, experiences a delayed (advanced) monsoon onset (retreat) by about 10–15 days, as shown in Fig. 2. Smith et al. (2008) also showed a shorter rainy season for northern Australia with traditional El Niño events.

Generally the monsoon onset date over Australia has a larger spread than the retreat. For instance, Smith et al. (2008) showed that the onset of the monsoon in northern Australia varied by 72 days in contrast to 25 days at the end of the rainy season. We find this result to be robust, despite our use of distinct datasets, regions, and time periods. The range between the earliest and the latest monsoon onset over the period 1979–2006 is 57 days and in the withdrawal 39 days for the region north of 20°S.

Smith et al. (2008) suggested that the level of humidity may be a determining factor in making the retreat of the monsoon more uniform than the onset. The increase of humidity at the start of the season is not the only factor to produce rain, but it is accompanied by a triggering event such as westerly wind bursts, tropical cyclones, storm systems, or the Madden–Julian oscillation (Wheeler and McBride 2005). At the end of the season, however, humidity decreases become less conducive to rainfall

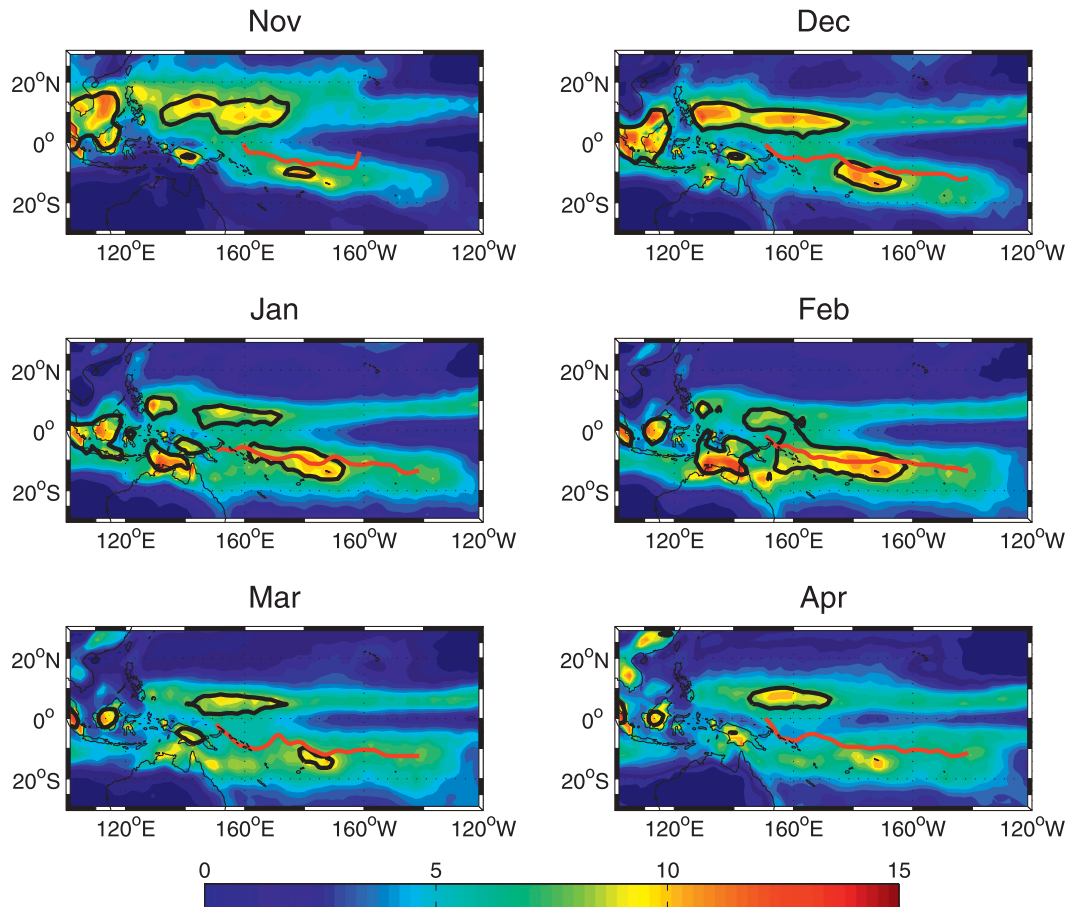


FIG. 3. Long-term monthly mean precipitation from NCEP–NCAR reanalysis from 1979 to 2005 during November–April. Areas within the solid black lines represent  $OLR < 220 \text{ W m}^{-2}$ . Red lines indicate the location of the maximum SST.

even in the presence of these triggering events. Although the difference in specific humidity between the start and the end of the monsoon cannot be clearly distinguished in Fig. 1g (black line) over the averaged northwestern Australian region, a significant reduction of humidity in December and March is noticeable during Modoki years (Fig. 1g, dashed line).

#### 4. The role of the convergence zones

The decrease in rainfall over northern Australia during Modoki events has been shown to be a response to anomalous subsidence generated by the double Walker circulation (Ashok et al. 2007; Wang and Hendon 2007; Taschetto and England 2009; Trenberth and Smith 2009). Taschetto et al. (2009) showed that the rainfall increase in February seen during Modoki events is due to a convergence of moisture associated with an anomalous cyclonic circulation over northern Australia. However, the

cause for this anomalous circulation in February has not been explained yet. The fact that the intensified rainfall over Australia occurs during the peak of the monsoon suggests that the atmospheric background state may play an important role in phase locking this response.

It is well known that the South Pacific convergence zone (SPCZ) is strongest during the southern summer months, particularly January–February (e.g., Vincent 1994). In addition, the intertropical convergence zone (ITCZ) reaches its southernmost position in February, merging with the SPCZ in the west Pacific over the warm pool. Therefore, we examine the seasonal evolution in precipitation, OLR, and SST to locate regions with strong convective activity as an estimate for the convergence zones.

Figure 3 presents the climatological rainfall, the regions with  $OLR < 220 \text{ W m}^{-2}$ , and the location of the maximum SST in the west tropical Pacific. It is clear that, during February, the west Pacific receives more

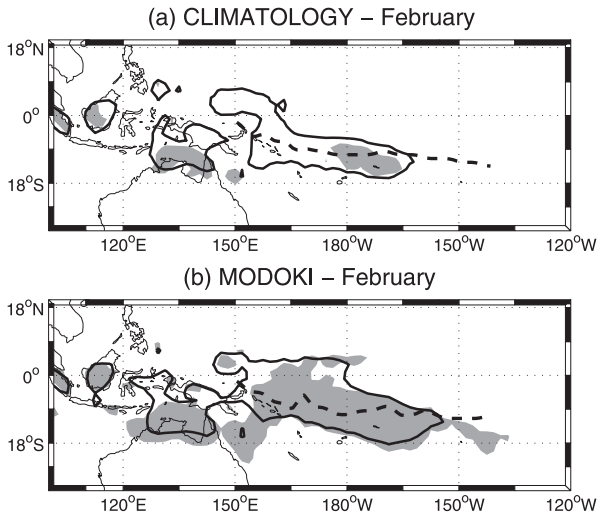


FIG. 4. As in Fig. 3, but for (a) February only and (b) for the composited Modoki events. Areas with precipitation larger than  $10 \text{ mm day}^{-1}$  are shaded. Areas within the solid black lines represent  $\text{OLR} < 220 \text{ W m}^{-2}$ . Dashed lines indicate the location of the maximum SST.

precipitation at the southern latitudes than during the other months. Associated with the region of heavy rainfall, there is a band of minimum OLR indicating areas with deep convective processes. Areas with strong deep convection are substantially reduced in the southern latitudes from April to November and enhanced in the northern latitudes of the west Pacific. The climatological fields in Fig. 3 are consistent with observed rainfall from CMAP (Xie and Arkin 1996) and OLR from the National Oceanic and Atmospheric Administration (NOAA) interpolated OLR dataset (Liebmann and Smith 1996). Interestingly, the maximum precipitation band consistently lies to the south of the axis of maximum SST. Although the zonally oriented portion of the SPCZ is tied to the region of maximum SST, the same cannot be said for its diagonal component. Kiladis et al. (1989) showed that the surface convergence maximum associated with the SPCZ is located to the south of the maximum precipitation band that in turn lies southward of the axis of maximum SST. Pressure gradients created by differences in SST drive low-level winds, which lead to moisture convergence where SST gradients are greatest (Vincent 1994).

Figure 4 focuses on the key month of February and allows a comparison between the climatological values and the conditions during Modoki events. The band of strong rainfall over the southwest Pacific is intensified during Modoki episodes (Fig. 4b). Similarly, precipitation over northern Australia is substantially strengthened. Furthermore, the area with minimum OLR is enhanced, suggesting stronger deep convection compared to the climatological values in February.

Deep convection processes can cause disturbances in the high troposphere generating a propagation of atmospheric waves. Generally, deep convection occurs more frequently as SST increases and is more intense over warmer regions. However, the link between warm underlying SST and the occurrence of deep convection is not direct. Strictly speaking, deep convection is dependent on low-to-midtropospheric moisture (Sherwood 1999), which in turn is more closely related to surface moisture convergence and atmospheric instability than SST (Khalsa 1983). Convergence at the surface supplies moisture that, together with turbulent heat fluxes into the atmosphere from the warm sea surface, provides ideal conditions for deep convection. We hypothesize that the anomalous warm sea surface in the central west Pacific during Modoki years in conjunction with the climatological convergence of moisture from the SPCZ intensifies the convective activity over the region. This generates wave disturbances in the higher troposphere. To show that enhanced deep convection occurs primarily in February compared to other months over the southern latitudes of the central west Pacific, we examine the relationship between SST, OLR, and precipitation in the next section.

## 5. Relationship between SST, OLR, and precipitation

In Fig. 5, we show the relationship between SST and convective processes in the tropical Pacific using OLR and precipitation as proxies for deep convection. This is a common approach to examine an SST threshold for the occurrence of deep convection processes (e.g., Graham and Barnett 1987; Bomventi et al. 2006). Each dot in Fig. 5a represents the OLR, SST, and rainfall data at a particular grid point and for a particular month at the tropical Pacific over the period 1979–2005.

A noticeable feature in Fig. 5a at any of the regions is the lack of rainfall associated with high values of OLR, as expected over clear-sky regions. However, a few grid points in the tropical Pacific (Fig. 5a) show low values of OLR associated with relatively low SST and no rainfall. Those points are associated with high, nonconvective clouds, such as cirrus, which are a product of deep convection probably generated over regions of warm land surface (e.g., Amazon basin). They are commonly observed in the east Pacific over relatively cool waters.

Although SST can influence deep convection, this link is indirect and depends on other factors. This is clear from the large variability of OLR over warmer waters shown in Fig. 5a. As previously mentioned, the large-scale surface moisture convergence induced by the SST gradient is a crucial factor (Kiladis et al. 1989). That is one of the reasons why deep convection is achieved

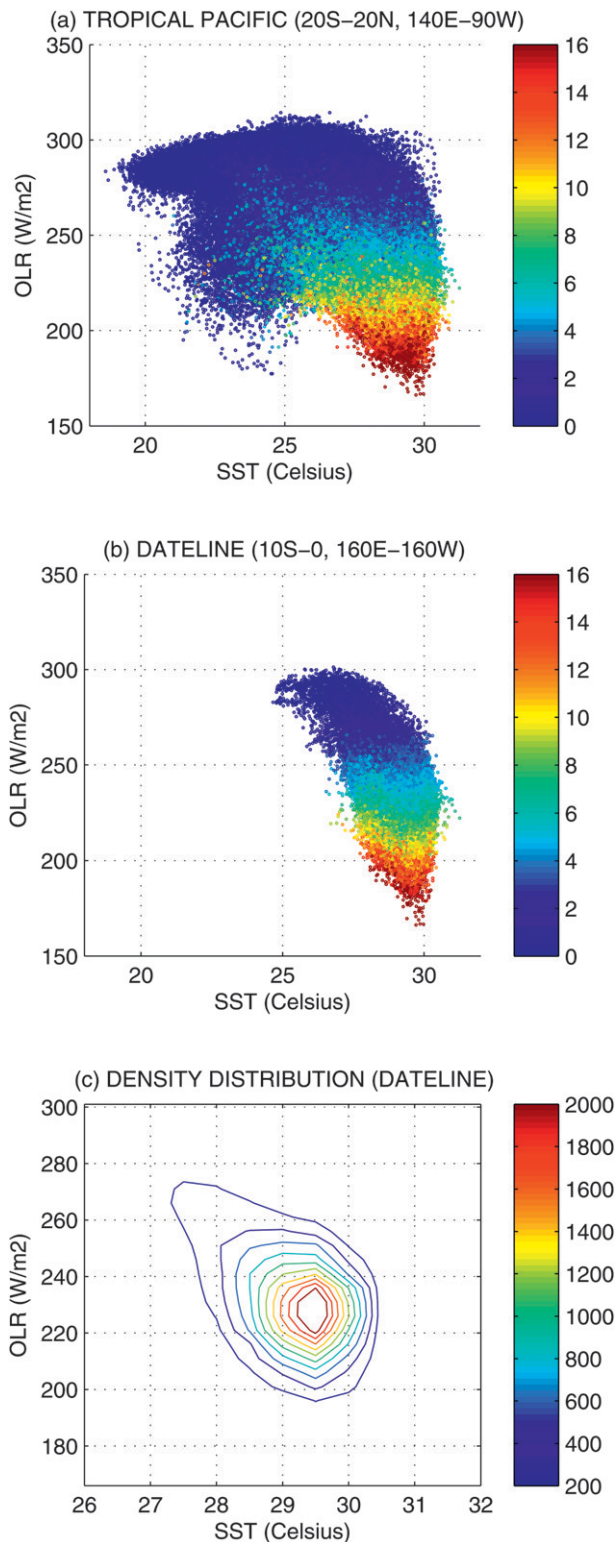


FIG. 5. Scatterplot of gridpoint monthly mean SST ( $^{\circ}\text{C}$ ) and OLR ( $\text{W m}^{-2}$ ) based on the period 1979–2005 for the (a) tropical Pacific ( $20^{\circ}\text{S}$ – $20^{\circ}\text{N}$ ,  $140^{\circ}\text{E}$ – $90^{\circ}\text{W}$ ) and (b) the southern tropical Pacific region around the date line, i.e.,  $0^{\circ}$ – $10^{\circ}\text{S}$ ,  $160^{\circ}\text{E}$ – $160^{\circ}\text{W}$ . Colors represent the rainfall intensity ( $\text{mm day}^{-1}$ ). (c) Density distribution of OLR for each SST in  $0.5^{\circ}\text{C}$  bins and OLR in  $5 \text{ W m}^{-2}$  bins for the date line region. Colored contours represent the number of observations.

more easily in the east Pacific than in the west. The lowest values of OLR and intense rainfall in the cold pool are associated with SST of approximately  $28^{\circ}\text{C}$ , while the warm pool is around  $29.5^{\circ}\text{C}$  (figure not shown). The surface wind convergence induced by SST gradients is much stronger in the east than in the west Pacific, where the SST is higher but exhibits less spatial variation. As a result, deep convection is more likely to occur in the east Pacific than over the warm-pool region for the same SST. As winds are generally weaker in the west because of the weaker SST gradients, anomalous wind convergence together with anomalous high SST constitutes an essential factor for inducing deep convection there (Deser and Wallace 1990).

Perhaps the most important information from Fig. 5 is that the relationship between OLR and SST is not linear. This behavior is evident in Fig. 5b for the Southern Hemisphere tropic region straddling the date line. This seems to be a key area of SST warming that affects the Australian monsoon during Modoki events, based on Taschetto et al. (2009) and Figs. 3 and 4. The OLR varies much less for SST below  $27^{\circ}\text{C}$ , but above this value, OLR decays steeply from  $300 \text{ W m}^{-2}$  to values below  $200 \text{ W m}^{-2}$ , reaching a minimum for temperatures between  $28^{\circ}$  and  $30^{\circ}\text{C}$ . Interestingly, the minimum OLR is not at the maximum SST. This is consistent with the fields shown in Figs. 3 and 4, where the line of maximum SST does not align with the maximum precipitation and minimum OLR. Zhang (1993) shows that deep convection is rarely observed for SST below  $26^{\circ}\text{C}$ , increases from  $26^{\circ}\text{C}$  up to  $29.5^{\circ}$ – $30^{\circ}\text{C}$ , and then decays for SST above  $30^{\circ}\text{C}$ .

To find an optimum value of SST associated with deep convection for the region around the date line, Fig. 5c shows the probability distribution of OLR for SST in  $0.5^{\circ}\text{C}$  bins and OLR in  $5 \text{ W m}^{-2}$  bins. The contours indicate the number of observations for each month at each individual binned grid point, as in a two-dimensional frequency histogram. In the central west Pacific at the southern latitudes around the date line, about 50% of the data with rainfall over  $3 \text{ mm day}^{-1}$  lie between  $29^{\circ}$ – $30^{\circ}\text{C}$  and  $220$ – $235 \text{ W m}^{-2}$ . In this region, the OLR is most likely to be observed around  $225 \text{ W m}^{-2}$  and associated with SST values around  $29.5^{\circ}\text{C}$ . This result corroborates the findings of Zhang (1993).

To investigate the variations of deep convection during the year, we show the monthly evolution (November–April) of the SST and OLR around the date line in Fig. 6. Convection strengthens in the austral summer and weakens significantly from April to July (not shown), with rare events where OLR is lower than  $200 \text{ W m}^{-2}$ . This behavior is consistent with Fig. 3. The largest variations in OLR occur from December to March, with values as high

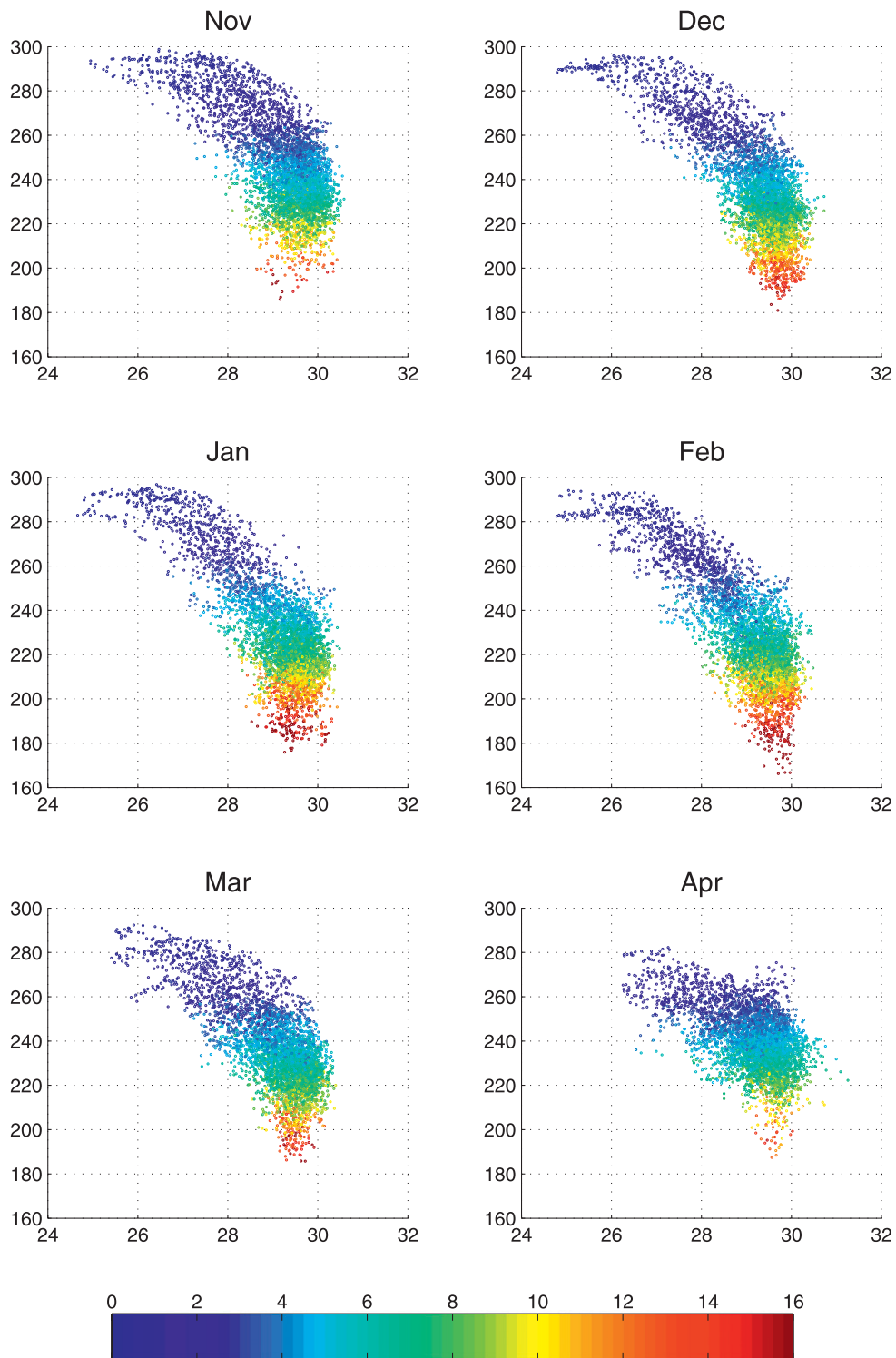


FIG. 6. Scatterplot of gridpoint monthly mean SST and OLR of the monthly means based on the period 1979–2005 for the southern tropical Pacific region around the date line, i.e., 0°–10°S, 160°E–160°W. Colors represent rainfall intensity ( $\text{mm day}^{-1}$ ).

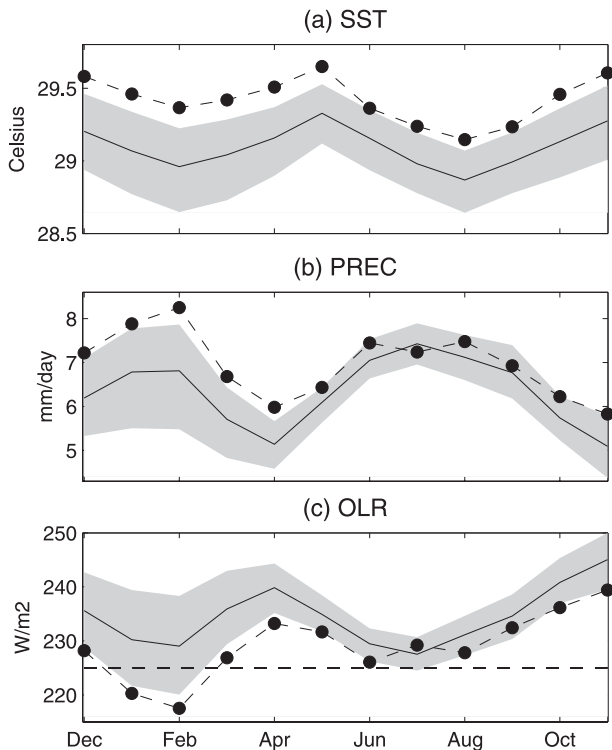


FIG. 7. Annual cycles of SST, precipitation, and OLR based on all years (solid lines) and Modoki years (dashed circle lines) for the averaged southern tropical Pacific region around the date line, i.e.,  $0^{\circ}$ – $10^{\circ}$ S,  $160^{\circ}$ E– $160^{\circ}$ W. The dashed line in (c) represents the OLR optimum value ( $225 \text{ W m}^{-2}$ ) obtained from Fig. 5c. Values outside the gray areas are statistically significant at the 95% confidence level based on a Monte Carlo test.

as  $300 \text{ W m}^{-2}$  and lower than  $200 \text{ W m}^{-2}$ . Minimum values of OLR are observed in February associated with the heaviest rainfall (more than  $20 \text{ mm day}^{-1}$ ) over the entire period 1979–2005. This suggests that there is a preference for the occurrence of deep convection over the central west Pacific around the date line in February. This again confirms the hypothesis that February is the month when intense deep convective processes occur more frequently and consequently generate the largest disturbances in the higher troposphere.

The seasonal cycles of SST, OLR, and precipitation for all the years and Modoki years averaged over the region of  $10^{\circ}$ S to the equator from  $160^{\circ}$ E to  $160^{\circ}$ W are shown in Fig. 7. The climatological SST reveals a semi-annual cycle with a range of about  $0.5^{\circ}\text{C}$  (Fig. 7a). The semiannual oscillation is also reflected in the climatology of precipitation and of OLR (Figs. 7b and 7c). The SST peaks in May and November and decreases to minimum values in February and August. Interannual variations in SST can be as large as the changes that occur between seasons. For instance, during Modoki events, the SST anomalies around the date line show, on

average, an increase of the same magnitude as the range of the climatological annual cycle. The composited annual cycle for Modoki events depicts a uniform upward shift of the SST throughout the year (Fig. 7a).

Interestingly, despite the consistent SST warming across all months during Modoki years, the response in rainfall and OLR is preferentially affected in the first half of the year. The largest increase in precipitation is observed in February, which agrees with the results shown in the previous sections. Rainfall around the date line is enhanced by approximately  $1.5 \text{ mm day}^{-1}$  in February during Modoki events (Fig. 7b).

The heavy rainfall is a consequence of the enhanced deep convection processes occurring in February, as observed from the OLR annual cycle (Fig. 7c). The largest difference between the climatology and the cycle composited during Modoki years also occurs in February when OLR declines by more than  $10 \text{ W m}^{-2}$ . The OLR in February during Modoki events drops below the threshold of  $220 \text{ W m}^{-2}$  in the monthly mean (Fig. 7c).

As shown in Fig. 5c, there is a preference for deep convection to occur with SST around  $29.5^{\circ}\text{C}$  and OLR of approximately  $225 \text{ W m}^{-2}$ . This is also evident in Fig. 7, where sufficiently low OLR values only occur in January and February (below the dashed line), when the SST is not necessarily at its maximum, but it is close to the optimum value.

As mentioned earlier, the link between SST and deep convection is indirect. The southward displacement of the ITCZ and the strengthening of the SPCZ in the southern summer months are conducive for the development of increased deep convection and heavy rainfall in the central west Pacific. However, during Modoki years, the warmer than normal SST in the central west Pacific enhances the supply of latent heat flux to the moist mixing layer. The anomalous convergence of winds at low levels and consequent rising motion due to conservation of mass, leads to anomalously enhanced vertical transport of moisture from the convective mixing layer to the midtroposphere, favoring the development of shallow and later deep convective clouds. Deep convection eventually leads to disturbances in the high troposphere generating a Gill–Matsuno-type response in the central west Pacific, as shown in the next section.

## 6. Diabatic heating and the Gill–Matsuno-type mechanism

### a. Observational evidence

According to thermodynamic theory, the vertical velocity of an air parcel is proportional to its diabatic heating [Eq. (1)]. In addition, any potential energy generated by diabatic heating is immediately converted to kinetic

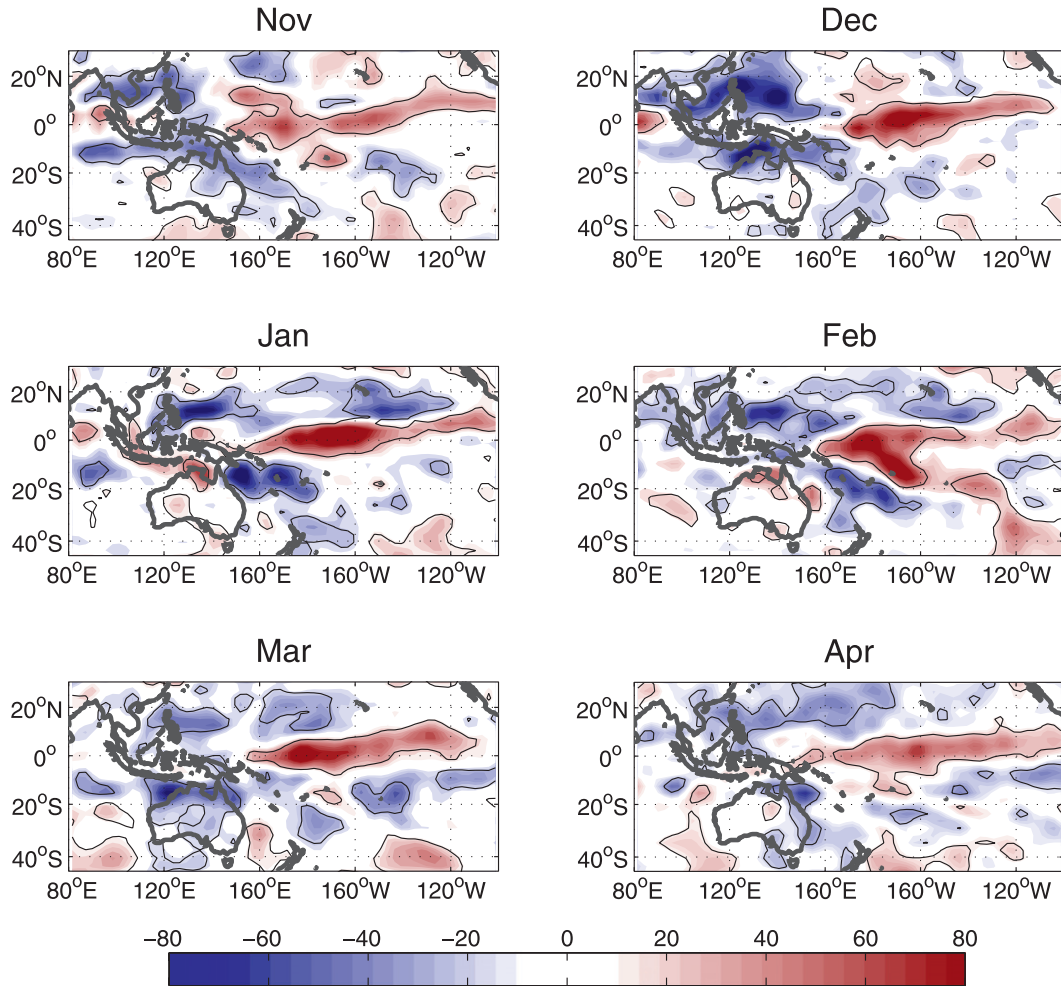


FIG. 8. Monthly anomalous diabatic heating ( $\text{W m}^{-2}$ ) during the composite Modoki events from November to April. Areas within the thin black contours are significant at the 0.05 significance level based on a Student's  $t$  test.

energy. Therefore, there is no storage in the form of available potential energy associated with atmospheric disturbances within the equatorial zone (Holton 1992).

A priori, the diabatic heating  $Q$  can be estimated from the thermodynamic equation (Trenberth and Solomon 1994):

$$c_p \left[ \frac{\partial T}{\partial t} + \mathbf{v} \cdot \nabla T + \omega \left( \frac{\partial T}{\partial p} - K \frac{T}{p} \right) \right] = Q, \quad (1)$$

where  $c_p$  is the specific heat capacity,  $\mathbf{v}$  is the velocity field,  $T$  is the temperature,  $\omega$  is vertical velocity,  $K$  is the kinetic energy, and  $p$  is pressure. In practice, the calculation of the vertically integrated monthly mean diabatic heating contains several details that complicate the balance of the terms. For instance, Trenberth et al. (2002) discuss differences that arise in the divergence of

total energy if the vertical integral is performed prior to taking the monthly mean and vice versa. The authors also discuss imbalances that arise from different resolution grids, vertical coordinates, distinct time scales, in addition to other technical complications.

For simplicity, we use the vertically integrated diabatic heating from Trenberth (1997), calculated as a residual of the energy budget, that is, comprised of the sum of total energy tendency, the divergence of total energy, and the latent heating—see Trenberth (1997) and Trenberth and Stepaniak (2003) for derivations and details of the budget equations.

Figure 8 shows the anomalous vertically integrated diabatic heating from November to April during Modoki events. Generally speaking, the diabatic heating anomalies are similar to the anomalous rainfall field, as the main source of diabatic heating is known to come from latent

heat release, precipitation, and moist convection. It is clear that the diabatic heating is significantly enhanced in the tropical Pacific along the equator over the ITCZ. In February, however, the anomalous diabatic heating is extended southward to the Southern Hemisphere in a diagonal band to the central Pacific. In the same month, a decrease in diabatic heating is located south of the positive diagonal band. This dipole anomaly in diabatic heating is clearly seen in February, suggesting a north-eastward shift of the SPCZ during Modoki events compared to its climatological mean position (Fig. 8). In addition, only during January and February is intensified diabatic heating found over northern Australia, consistent with increased rainfall during Modoki events.

Diabatic heating associated with precipitation in the tropics can generate a remote response in the atmosphere via excitation of equatorial waves. Gill (1980) used a simple analytical model to generalize a response of the tropical atmosphere to diabatic heating. The author based the model on the theory of Matsuno (1966) for the forced shallow-water equations in the tropics. Gill (1980) demonstrated that a symmetric heating centered on the equator induces a low-level easterly flow via propagation of Kelvin waves and a return flow in the west over a more limited region away from the equator and with faster decay. The return flow toward the equator is manifested as a cyclonic circulation over the low pressure systems that form on the western margins of the heating area as part of a Rossby wave. For a symmetric heating source about the equator, the cyclonic circulation develops in both hemispheres. If the diabatic heating is asymmetric about the equator, the cyclonic circulation is enhanced in the hemisphere with greater heating and a smaller anticyclonic circulation appears in the opposite hemisphere. The Gill–Matsuno-type response to diabatic heating can be identified by anomalous circulation at high and low levels of the atmosphere, for instance, by examining sea level pressure, streamfunction, and/or wind fields.

Figure 9a shows the vertically integrated moisture flux from the surface to 500 hPa and the associated divergence in February composited for Modoki events. Associated with the increased diabatic heating in the tropical Pacific is a convergence of winds and moisture around the date line and a cyclonic circulation to the west of the heating source, located over northern parts of Australia (Fig. 9a). A center of low sea level pressure is located over northwestern Australia (figure not shown), although it is not significant at the 0.05 significance level.

Figures 10 and 11 show the monthly evolution of observed anomalies of streamfunction at 100 and 850 hPa, respectively, composited for Modoki events. An alternating pattern in the anomalous streamfunction over

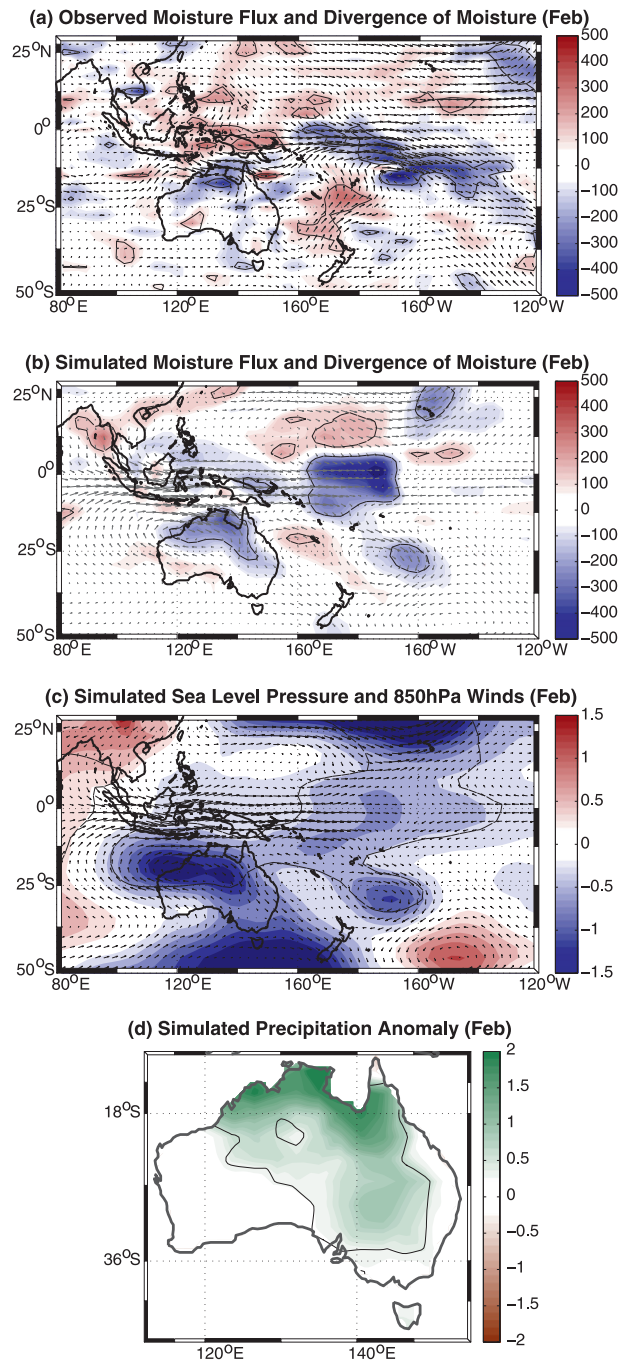


FIG. 9. (a) Anomalous moisture flux ( $\text{kg m}^{-1} \text{s}^{-1}$ , vectors) and divergent moisture flux ( $\text{kg s}^{-1}$ , shaded) vertically integrated from the surface to 500 hPa for (a) Modoki composites of observed February and (b) simulated February for the idealized experiment. (c) Simulated sea level pressure (hPa) and low-level winds ( $\text{m s}^{-1}$ ) and (d) simulated rainfall anomaly ( $\text{mm day}^{-1}$ ) in February for the idealized experiment. Maximum vector lengths are  $1.5 \text{ kg m}^{-1} \text{ s}^{-1}$  in (a) and (b) and  $4 \text{ m s}^{-1}$  in (c). Areas within thin black contours are significant at the 0.05 significance level based on a Student's  $t$  test.

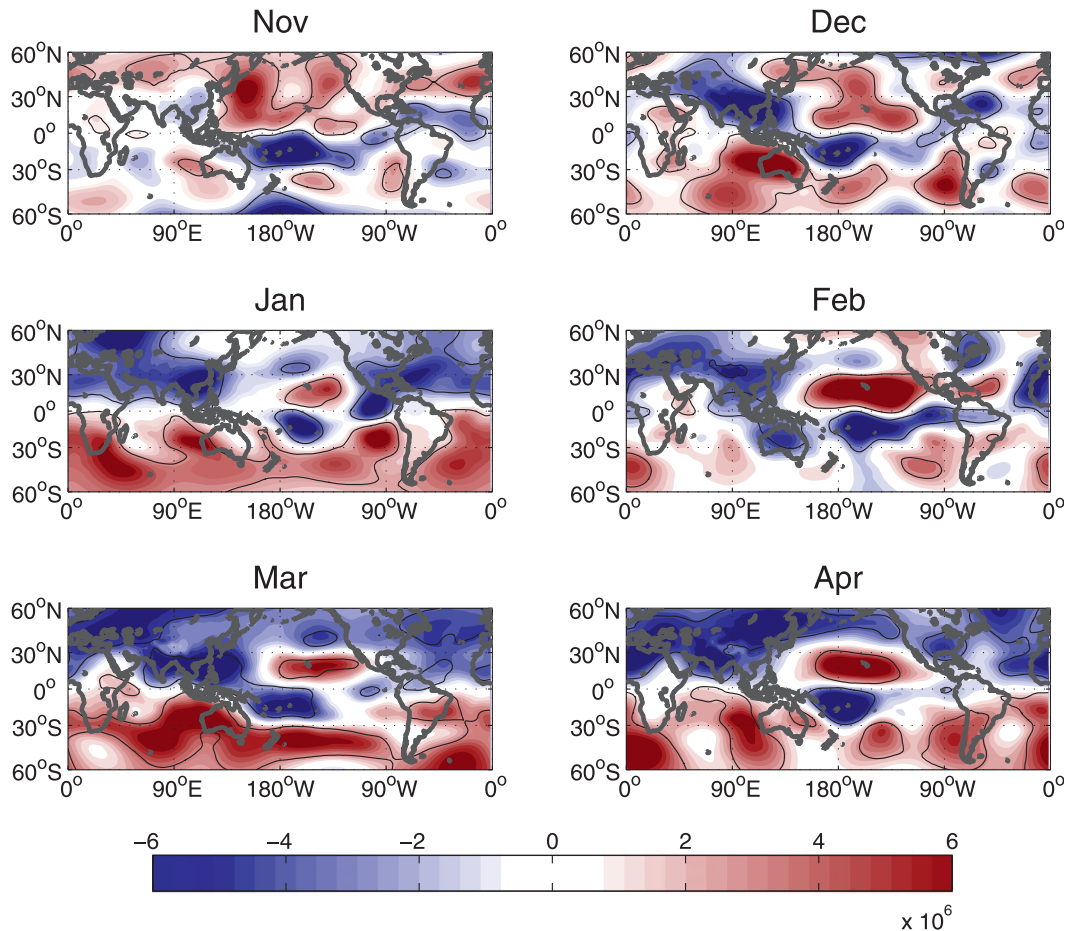


FIG. 10. Monthly observed streamfunction anomalies ( $\text{m}^2 \text{s}^{-1}$ ) at 100 hPa from November to April composited for Modoki events. Areas within the thin black lines are significant at the 0.05 significance level based on a Student's *t*-test.

the Pacific Ocean can be seen in the upper atmosphere from November to April (Fig. 10), suggesting the propagation of a Rossby wave train from the tropics to the extratropics in both hemispheres. Over Australia, the streamfunction anomaly at high levels of the atmosphere during February is negative, opposing the positive anomaly at low levels (Fig. 11, middle right) and the cyclonic circulation seen in Fig. 9a. This suggests a baroclinic response during Modoki events in February, consistent with Gill (1980)'s theory.

At the end of the monsoon (i.e., March), however, the mean winds reverse over the northern part of the continent and humidity starts to decrease across Australia as part of a typical monsoonal cycle (Fig. 1g). Deep convection in the tropical Pacific is reduced compared to January and February (Figs. 3, 6, and 7) and the SPCZ is weakened. The persistence of the SST warming in the tropical Pacific is not in itself sufficient to translate into the enhanced diabatic heating required to produce a

Gill response, or at least the return flow from the Gill–Matsuno theory is not located over Australia. Nonetheless, it still drives an atmospheric response associated with the anomalous double Walker cell described by Ashok et al. (2007). The western subsiding branch lies over Australian longitudes, inhibiting convection, the formation of clouds, precipitation, and consequently causing a divergence of moisture across the continent (Taschetto and England 2009; Taschetto et al. 2009).

As a proxy for the anomalous Walker circulation, we assess the velocity potential anomaly field at 100 hPa composited during Modoki years (Fig. 12). Positive (negative) values of velocity potential indicate convergence (divergence) at high levels generally associated with subsidence (upward motion) throughout the troposphere. The strongest anomalies are located in the equatorial Pacific around the date line, reinforcing our hypothesis that this is a key region during Modoki events for the modulation of Australian rainfall. The double

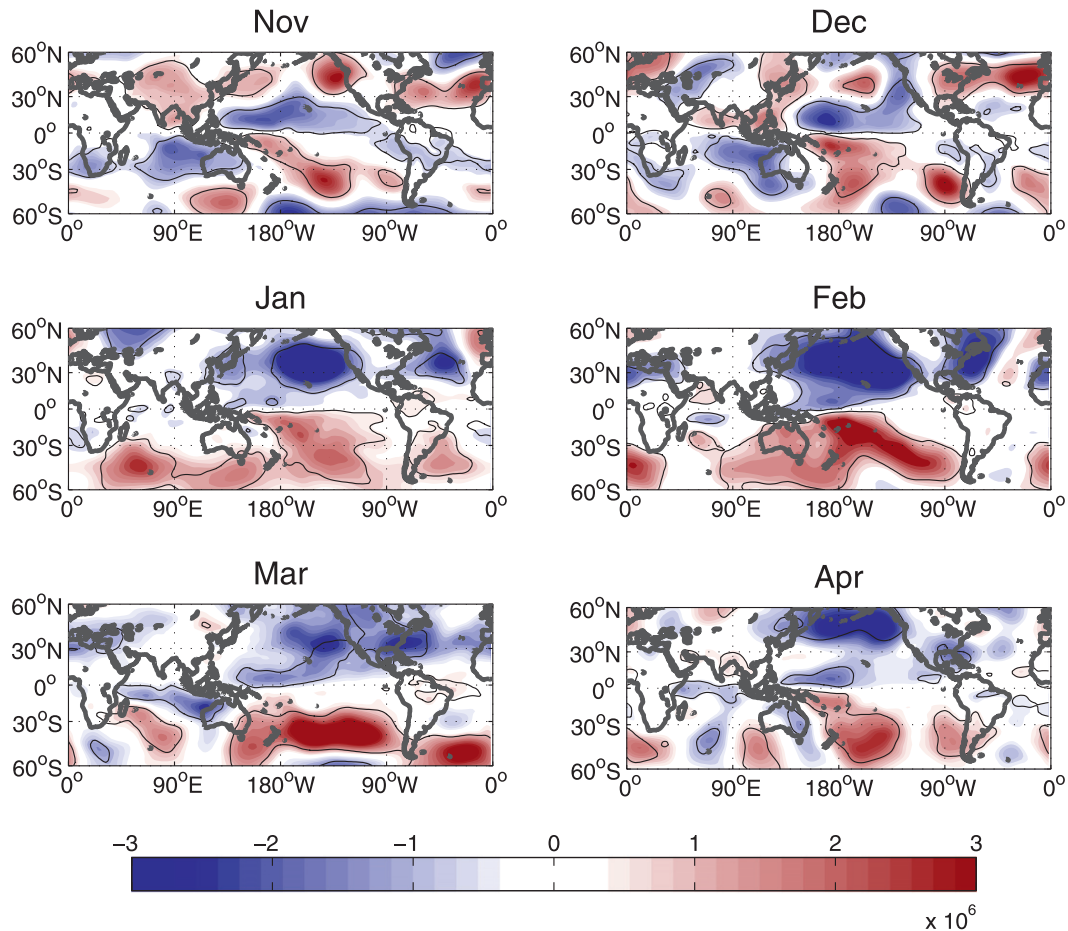


FIG. 11. As in Fig. 10, but at 850 hPa.

Walker cell associated with Modoki events is clearly identified during November and December. In these months, low-level wind convergence and uplift take place over anomalously warm SST in the central west tropical Pacific and subsiding branches are located over South America and Australia. In the ensuing months, that is, January to April, rising motion is also seen over the Pacific; however, the eastern branch of the double Walker cell is no longer clear over South America. Over Australia, subsidence is evident from November to April, except during the peak of the monsoon (i.e., January and February). The subsidence over Australia during December and March is consistent with the reduction of rainfall shown in Figs. 1b and 1e. Despite strong uplift around the date line, Australia does not experience significant subsidence during January and February. At this time, a Gill–Matsuno-type response generates a cyclonic circulation anomaly over northwestern Australia, that in turn leads to increased rainfall over northwestern Australia during these 2 months (see also Figs. 1c and 1d). Thus, the observational

evidence shown in Figs. 9a and 10–12 confirm the hypothesis that during January and February the subsiding branch of the Walker circulation over Australia is overwhelmed by a Gill–Matsuno-type response during Modoki events.

#### b. Model experiments

The atmospheric response to the anomalous SST warming in the central west Pacific seen in observations is tested here with an AGCM experiment. A  $1^{\circ}\text{C}$  anomaly is superimposed on the SST seasonal cycle around the date line as shown in Fig. 1a. Based on the ensemble simulations, the SST warming in the central west Pacific generates a low-pressure anomaly over the forcing area (Fig. 9c). As a consequence, near-surface winds converge in the lower-pressure area, leading to enhanced air–sea latent heat flux and rising motion following the continuity equation. This anomalous rising motion intensifies the climatological updraft already present during February, advecting moisture to the troposphere and thus driving deep

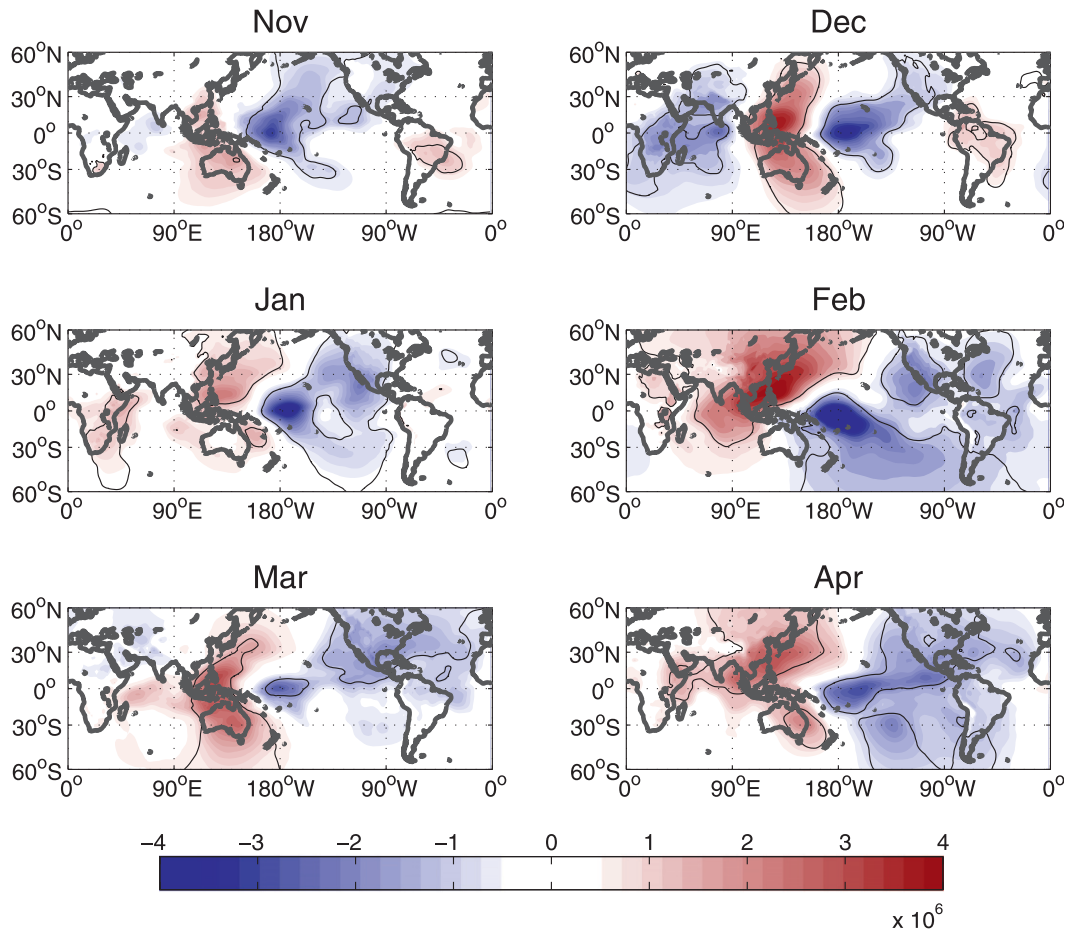


FIG. 12. Modoki composites of observed monthly velocity potential anomalies ( $\text{m}^2 \text{s}^{-1}$ ) at 100 hPa from November to April. Areas within the thin black lines are significant at the 0.05 significance level based on a Student's  $t$  test.

convection that eventually leads to an overall enhancement of the SPCZ.

The convergence of winds and moisture in conjunction with the anomalous heating in the SPCZ is displaced toward the Southern Hemisphere. This gives rise to a Gill–Matsuno-type response with a cyclonic circulation over Australia to the west of the SST forcing clearly seen both in the vertically integrated moisture flux (Fig. 9b) and in sea level pressure (Fig. 9c). The convergence of low-level winds and moisture associated with the anomalous cyclonic circulation favors a strengthening of the monsoon by the climatological westerlies over the northwestern Australia at this time of the year. As a result, intensified precipitation takes place over northern Australia in February during Modoki events. It is worth noting that the positive rainfall anomaly simulated during February (Fig. 9d) is larger than the observed because of a stronger anomalous circulation response to the tropical heating. Nonetheless, the similarities between the observed (Fig. 9a) and simulated (Fig. 9b)

moisture flux are impressive given the simplicity of the experiment.

At the upper levels of the atmosphere, the anomalous heating in the equatorial Pacific generates height perturbations associated with Rossby–gravity waves consistent with Matsuno (1966). This response manifests as a quadrupole vortex structure in the horizontal streamfunction at 100 hPa, with an upper-level ridge over Australia, as seen in Fig. 13a. At low levels, positive streamfunction anomalies at 850 hPa (Fig. 13b) and negative sea level pressure anomalies (Fig. 9c) appear over Australia indicating the baroclinic structure generated by the anomalous SST forcing in the central west Pacific. It is worth noting that the simulated streamfunction anomalies show a very clear pattern in response to the tropical heating imposed in the numerical experiment. A clear pattern is generally more difficult to observe in nature, as the existence of other forcings generates a much more complex pattern in the streamfunction anomalies (Figs. 10 and 11). Herein lies

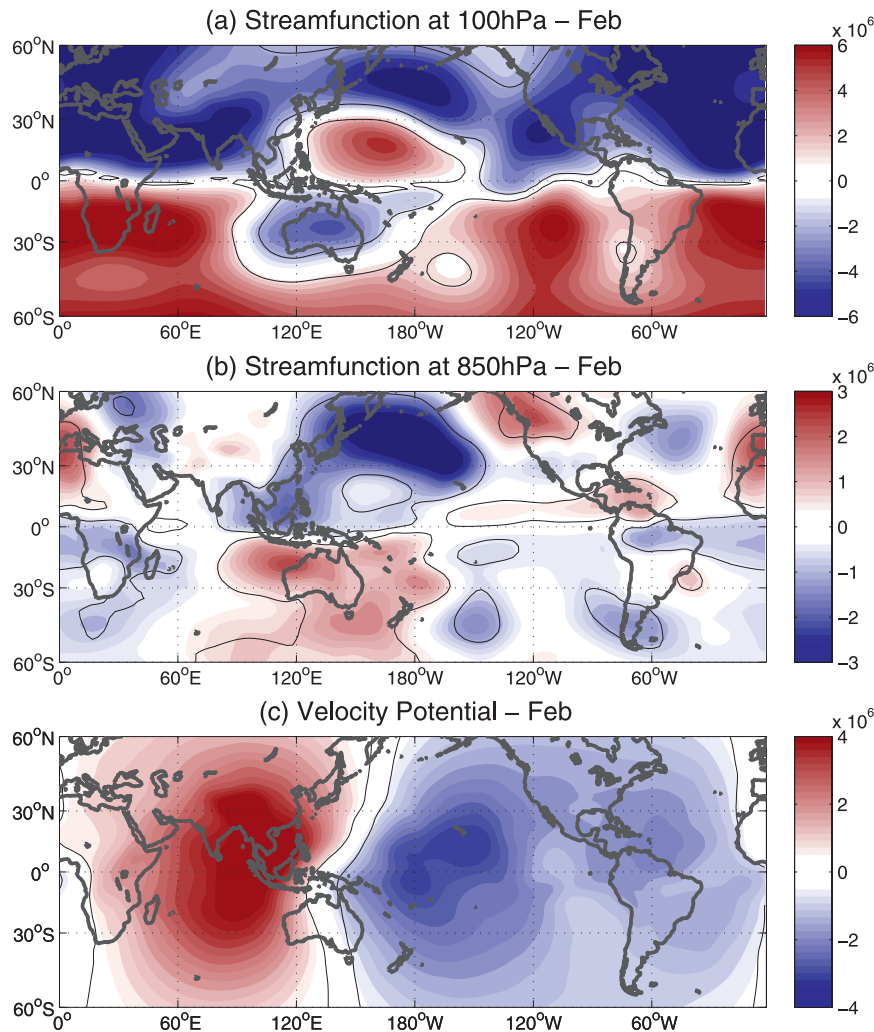


FIG. 13. Simulated anomalies of streamfunction ( $\text{m}^2 \text{s}^{-1}$ ) (a) at 100 and (b) 850 hPa and (c) velocity potential at 100 hPa ( $\text{m}^2 \text{s}^{-1}$ ) in February for the idealized experiment forced with an equatorial  $1^\circ\text{C}$  SST warming around the date line. Areas within the thin black lines are significant at the 0.05 significance level based on a Student's  $t$  test.

the importance of the AGCM experiments, because they help to identify the effect of a unique forcing, that is, the central west Pacific warming.

A clear displacement of the Walker circulation is simulated in February as seen by the anomalous velocity potential in Fig. 13c. Strong updrafts appear in the central west Pacific with a consequent downward motion located in the tropical Indian Ocean extending to midlatitudes over South Asia. This is consistent with the observed vertical velocity anomalies composited during Modoki events (Fig. 12), despite the shift of the maximum anomalies to Southeast Asia in the observations. Australia lies in between the velocity potential anomalies in February for both observations and simulations.

## 7. Summary and conclusions

In this study, we have examined the mechanisms that cause heavy precipitation during the peak of the Australian monsoon when combined with warming in the central west Pacific. In particular, we examine the post-1979 Modoki events identified by Ashok et al. (2007). Modoki events drive an anomalous Walker circulation whose western-subsiding branch lies over Australia, inhibiting convection, and resulting in below-average rainfall across the continent. This physical process dominates over Australia in all months, except during January and February, when intensified rainfall is generally observed. Taschetto et al. (2009) showed that the increased monsoonal precipitation over northern Australia occurs

due to a convergence of moisture associated with a cyclonic circulation. Such behavior is the opposite to that observed during traditional El Niño episodes, when Australia normally experiences dry conditions, in particular, during the peak of the monsoon associated with anomalous subsidence from the Walker circulation.

The reason why an anomalous cyclonic circulation appears over Australia during Modoki events has been unclear. Here, we extend the previous study by explaining that the anomalous convergent flow that takes place in February over northwestern Australia is in fact due to the westward propagation of a Rossby wave excited by a perturbation in the high troposphere as a result of tropical diabatic heating. This mechanism is consistent with the idealized theory suggested by Gill (1980). The generation of the Rossby wave to the west of the heating anomaly appears persistently only during the peak of the southern summer because of an interaction between the interannual variability and the climatological mean state. In other words, this atmospheric response over northern Australia is phased locked to the seasonal cycle.

The Gill–Matsuno response is already known to occur during conventional El Niño events. However, this mechanism has not been examined thus far for Modoki events. The Gill–Matsuno anomaly generally occurs during traditional El Niño episodes (e.g., Lee et al. 2009) because the SST anomalies in the east Pacific are much larger than in the central west during Modoki and deep convection occurs there over a relatively lower SST threshold than in the west. As the Modoki-related SST anomalies are not as high as those during traditional El Niños, they are not in themselves sufficient to significantly perturb the troposphere. Instead, they optimize conditions for enhanced deep convective processes that occur in the ITCZ and SPCZ regions. The southward shift of the ITCZ and the intensified SPCZ during the austral summer months not only enhance the Walker circulation anomaly during Modoki events, they are also essential to generating the remote Australian response via a Gill–Matsuno-type mechanism. The central west Pacific warming during Modoki events leads to enhanced convergence of winds and latent heat exchanges from the ocean to the atmosphere. In February, this response enhances the climatological conditions within the convective zone and intensifies the vertical transport of moist air, generating increased deep convection. This in turn causes disturbances in the upper troposphere akin to a Gill–Matsuno-type response to a heating about the equator. The anomalous diabatic heating generates a baroclinic response with the propagation of Rossby waves to northwestern Australia. This anomalous circulation enhances rainfall at the peak of the Australian monsoon, overwhelming the subsiding branch of the

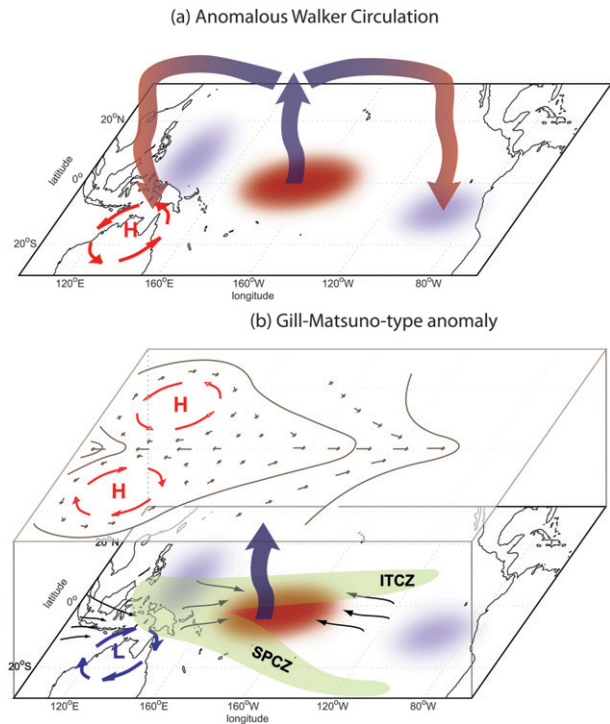


FIG. 14. Schematic of the atmospheric response during Modoki events when warm SST anomalies shift to the central west tropical Pacific. (a) The western-subsiding branch of the Walker circulation lies over Australia in December and March. (b) The intensification of the SPCZ in the austral summer months in conjunction with the anomalous warm waters enhances deep convection in January and February, generating high-level disturbances in a Gill–Matsuno-type mechanism. These two thermodynamic processes generate opposing responses over northern Australia—namely, (i) an anticyclonic circulation, divergence of moisture, and below-average rainfall conditions in December and March in (a), and (ii) cyclonic circulation, convergence of moisture, and enhanced precipitation during January and February in (b).

Walker cell during Modoki events. Figure 14 illustrates the atmospheric circulation that occurs in austral summer months during Modoki years.

Our observational analyses were confirmed here using an idealized experiment forced by a positive 1°C anomaly superimposed onto the SST seasonal cycle over the equatorial Pacific around the date line. A Gill–Matsuno horizontal quadrupole vortex structure appears at upper levels of the atmosphere, identified by the streamfunction anomaly at 100 hPa. The Gill–Matsuno quadrupole response has a distinct seasonality in our idealized experiment, with February containing the strongest anomalies. The simulated Gill–Matsuno response occurs during the entire austral summer months (i.e., December–February) in our numerical experiment (not shown). This seems to be related to the fact that the simulated SPCZ is already well developed in December,

whereas in observations it exhibits intensification in January.

The anomalous cyclonic circulation over northwestern Australia leads to an intensification of the climatological westerly winds that takes place during the monsoon in the southeast Indian Ocean and Indonesian seas. This leads to convergence of moisture fluxes over northwestern Australia that favors convection and thus enhances precipitation at the peak of the monsoon during the central west Pacific warm events.

The Gill–Matsuno mechanism of the heat-induced tropical circulation is clearly identified in our idealized AGCMs ensemble, but it is more difficult to discern in the actual atmosphere because of the interaction of the other heating sources. It would be worthwhile to identify the quadrupole structure in observations and to test the mechanism using other general circulation models.

It is worth noting that the observations show a clear northeastward displacement of the enhanced SPCZ during Modoki events, suggesting that the anomalous convergence of winds due to the low pressure created over the SST anomaly plays an important role in modulating the position of this convergence zone. The shift of the SPCZ during conventional El Niño events has been reported in the literature by several authors (e.g., Trenberth and Shea 1987; Vincent 1994). Our numerical experiment, however, does not show a strong shift of the SPCZ with SST warming over the central west Pacific. This may be related to the fact that the normal position of the subtropical convergence zones in AGCMs is generally biased toward the north, relative to the observations. In particular, the structure of the SPCZ is slightly zonal in CAM3 (Hack et al. 2006), a bias also present in several other general circulation models (Randall et al. 2007).

It is important to note that this study makes use of a simple AGCM experiment. Zhou et al. (2009) show that the circulation associated with the Asian–Australian monsoon system is captured relatively well by AGCM experiments; however, they fail in reproducing rainfall anomalies. Here, we show that an idealized SST forcing in an AGCM is able to produce both the circulation and rainfall anomalies over northern Australia, consistent with those observed in February during El Niño Modoki events. However, the Australian monsoon system also depends on other important factors not assessed here, for instance, the possible role of feedbacks involving the SST and winds around the Maritime Continent and local rainfall. A possible feedback may take place in the region as described by Hendon (2003). The westerly wind anomalies north of Australia that occur during Modoki events could potentially enhance the monsoon by intensifying the cyclonic circulation resulting from the Gill–Matsuno mechanism in February (Fig. 9). However,

a possible weakening of the monsoon can also occur. During Modoki events, the waters north of Australia tend to be colder than average. The westerly anomalies north of Australia could act to increase the mean wind speed, which are normally westerly/northwesterly at this time of the year. Consequently, this could cool the underlying SST even more by changing the air–sea fluxes. The cold SST, in turn, could act to weaken the Australian monsoon by reducing the strength of the anomalous cyclonic circulation and rainfall via inhibiting local convection. The damping effect from the cold SST anomalies may be one of the reasons why the anticyclone over northern Australia appears weaker in observations than in the simulations with no feedbacks.

It is also likely that the cool SST anomalies north of Australia that accompany the Modoki pattern have a different local effect on the monsoon circulation. The relatively cool waters around the Maritime Continent could intensify the monsoonal rainfall over northern Australia by enhancing the pressure gradient between ocean and land. The cross-equatorial moisture flux anomaly from the Maritime Continent to the area of anomalous warm SST is larger in the observations than in the simulations (Figs. 9a and 9b), suggesting that a positive feedback may be occurring in the region. On the other hand, additional experiments forced with an idealized Modoki pattern (i.e., cool waters on both sides of the Pacific and warming in the central basin) showed a reduced rainfall response over northwestern Australia compared to the central western experiment, suggesting a negative feedback between the Gill–Matsuno response and local convection. The contribution of the local feedback to Australian rainfall remains an open question.

Sea surface temperature variability in the tropical Pacific is one of the major drivers of Australian rainfall variations. A better understanding of how different flavors of El Niño impact global and regional climate is therefore fundamental to improving the predictive skill for Australian rainfall. The results obtained in this study show that warmer than average waters in the central west tropical Pacific modulate the Australian monsoon, not only via a shift in the Walker circulation, but also via a Gill–Matsuno-type response in the atmosphere.

*Acknowledgments.* This research was supported by the Australian Research Council. The NCEP–NCAR reanalysis and NCEP reanalysis 2 data were provided by the NOAA/OAR/ESRL PSD, Boulder, Colorado, from their Web site (available online at <http://www.esrl.noaa.gov/psd/>). The HadISST was provided by the Met Office Hadley Centre. The budget products derived

from the NCEP–NCAR reanalysis were obtained online from <http://www.cgd.ucar.edu/cas/catalog/newbudgets/index.html>. Use of NCAR's CCSM3 model is gratefully acknowledged. The model simulations were run at the Australian Partnership for Advanced Computing National Facility. We thank the anonymous reviewers for their comments that led to improvements in the manuscript.

## REFERENCES

- Arblaster, J. M., G. A. Meehl, and A. M. Moore, 2002: Interdecadal modulation of Australian rainfall. *Climate Dyn.*, **18**, 519–531.
- Ashok, K., S. K. Behera, S. A. Rao, H. Weng, and T. Yamagata, 2007: El Niño Modoki and its possible teleconnection. *J. Geophys. Res.*, **112**, C11007, doi:10.1029/2006JC003798.
- Bomventi, T. N., I. Wainer, and A. S. Taschetto, 2006: Relação entre a radiação de onda longa, precipitação e temperatura da superfície do mar no Oceano Atlântico Tropical (in Portuguese). *Braz. J. Geophys.*, **24**, 513–524.
- Branstator, G., 1985: Analysis of general circulation model sea surface temperature anomaly simulations using a linear model. Part I: Forced solutions. *J. Atmos. Sci.*, **42**, 2225–2241.
- Collins, W. D., and Coauthors, 2004: Description of the NCAR Community Atmosphere Model (CAM 3.0). National Center for Atmospheric Research Rep. NCAR/TN-464+STR, 226 pp.
- Deser, C., and J. M. Wallace, 1990: Large-scale atmospheric circulation features of warm and cold episodes in the tropical Pacific. *J. Climate*, **3**, 1254–1281.
- Gill, A. E., 1980: Some simple solutions for heat-induced tropical circulation. *Quart. J. Roy. Meteor. Soc.*, **106**, 447–462.
- Graham, N. E., and T. P. Barnett, 1987: Sea surface temperature, surface wind divergence, and convection over tropical oceans. *Science*, **238**, 657–659.
- Hack, J. J., J. M. Caron, S. G. Yeager, K. W. Oleson, M. M. Holland, J. E. Truesdale, and P. J. Rasch, 2006: Simulation of the global hydrological cycle in the CCSM Community Atmosphere Model version 3 (CAM3): Mean features. *J. Climate*, **19**, 2199–2221.
- Hendon, H. H., 2003: Indonesian rainfall variability: Impacts of ENSO and local air–sea interaction. *J. Climate*, **16**, 1775–1790.
- Holton, J. R., 1992: *An Introduction to Dynamic Meteorology*. 3rd ed. Academic Press, 511 pp.
- Kalnay, E., and Coauthors, 1996: The NCEP/NCAR 40-Year Reanalysis Project. *Bull. Amer. Meteor. Soc.*, **77**, 437–471.
- Kanamitsu, M., W. Ebisuzaki, J. Woollen, S.-K. Yang, J. J. Hnilo, M. Fiorino, and G. L. Potter, 2002: NCEP–DOE AMIP-II Reanalysis (R-2). *Bull. Amer. Meteor. Soc.*, **83**, 1631–1643.
- Khalsa, S. J. S., 1983: The role of the sea surface temperature in large-scale air–sea interaction. *Mon. Wea. Rev.*, **111**, 954–966.
- Kiladis, G. N., S. von Storch, and H. van Loon, 1989: Origin of the South Pacific Convergence Zone. *J. Climate*, **2**, 1185–1195.
- Kim, H.-M., P. J. Webster, and J. A. Curry, 2009: Impact of shifting patterns of Pacific Ocean warming on North Atlantic tropical cyclones. *Science*, **325**, 77–80.
- Kumar, K. K., B. Rajagopalan, M. Hoerling, G. Bates, and M. Cane, 2006: Unraveling the mystery of Indian monsoon failure during El Niño. *Science*, **314**, 115–119.
- Larkin, N. K., and D. E. Harrison, 2005: On the definition of El Niño and associated seasonal average U.S. weather anomalies. *Geophys. Res. Lett.*, **32**, L16705, doi:10.1029/2005GL022738.
- Lavery, B., A. Kariko, and N. Nicholls, 1992: A historical rainfall data set for Australia. *Aust. Meteor. Mag.*, **40**, 33–39.
- Lee, S.-K., C. Wang, and B. A. Mapes, 2009: A simple atmospheric model of the local and teleconnection responses to tropical heating anomalies. *J. Climate*, **22**, 272–284.
- Liebmann, B., and C. A. Smith, 1996: Description of a complete (interpolated) outgoing longwave radiation dataset. *Bull. Amer. Meteor. Soc.*, **77**, 1275–1277.
- Luo, J.-J., S. Masson, S. K. Behera, and T. Yamagata, 2008: Extended ENSO predictions using a fully coupled ocean–atmosphere model. *J. Climate*, **21**, 83–93.
- Matsuno, T., 1966: Quasi-geostrophic motions in the equatorial area. *J. Meteor. Soc. Japan*, **44**, 25–43.
- Nicholls, N., 1984: The Southern Oscillation, sea-surface temperature, and interannual fluctuations in Australian tropical cyclone activity. *Int. J. Climatol.*, **4**, 661–670.
- Randall, D. A., and Coauthors, 2007: Climate models and their evaluation. *Climate Change 2007: The Physical Science Basis*, S. Solomon et al., Eds., Cambridge University Press, 589–662.
- Rayner, N. A., D. E. Parker, E. B. Horton, C. K. Folland, L. V. Alexander, D. P. Rowell, E. C. Kent, and A. Kaplan, 2003: Global analyses of SST, sea ice and night marine air temperature since the late nineteenth century. *J. Geophys. Res.*, **108**, 4407, doi:10.1029/2002JD002670.
- Sherwood, S., 1999: Convective precursors and predictability in the tropical western Pacific. *Mon. Wea. Rev.*, **127**, 2977–2991.
- Smith, I. N., L. Wilson, and R. Suppiah, 2008: Characteristics of the Northern Australian rainy season. *J. Climate*, **21**, 4298–4311.
- Suppiah, R., 1992: The Australian summer monsoon: A review. *Prog. Phys. Geogr.*, **16**, 283–318.
- Taschetto, A. S., and M. H. England, 2009: El Niño Modoki impacts on Australian rainfall. *J. Climate*, **22**, 3167–3174.
- , C. C. Ummenhofer, and A. S. G. M. H. England, 2009: The effect of anomalous warming in the central Pacific on the Australian monsoon. *Geophys. Res. Lett.*, **36**, L12704, doi:10.1029/2009GL038416.
- Trenberth, K. E., 1997: Using atmospheric budgets as a constraint on surface fluxes. *J. Climate*, **10**, 2796–2809.
- , and D. J. Shea, 1987: On the evolution of the Southern Oscillation. *Mon. Wea. Rev.*, **115**, 3078–3096.
- , and A. Solomon, 1994: The global heat balance: Heat transports in the atmosphere and ocean. *Climate Dyn.*, **10**, 107–134.
- , and D. P. Stepaniak, 2001: Indices of El Niño evolution. *J. Climate*, **14**, 1697–1701.
- , and —, 2003: Co-variability of components of poleward atmospheric energy transports on seasonal and interannual timescales. *J. Climate*, **16**, 3690–3704.
- , and L. Smith, 2009: Variations in the three-dimensional structure of the atmospheric circulation with different flavors of El Niño. *J. Climate*, **22**, 2978–2991.
- , D. P. Stepaniak, and J. M. Caron, 2002: Interannual variations in the atmospheric heat budget. *J. Geophys. Res.*, **107**, 4066, doi:10.1029/2000JD000297.
- Vincent, D. G., 1994: The South Pacific Convergence Zone (SPCZ): A review. *Mon. Wea. Rev.*, **122**, 1949–1970.
- Wang, G., and H. H. Hendon, 2007: Sensitivity of Australian rainfall to inter-El Niño variations. *J. Climate*, **20**, 4211–4226.
- Weng, H., K. Ashok, S. K. Behera, S. A. Rao, and T. Yamagata, 2007: Impacts of recent El Niño Modoki on dry/wet conditions in the Pacific rim during boreal summer. *Climate Dyn.*, **29**, 113–129.
- Wheeler, M. C., and J. L. McBride, 2005: Australian–Indonesian monsoon. *Intraseasonal Variability in the Atmosphere–Ocean*

- Climate System*, W. K. M. Lau, Ed., Springer Berlin Heidelberg, 125–173.
- Xie, P., and P. A. Arkin, 1996: Analyses of global monthly precipitation using gauge observations, satellite estimates, and numerical model predictions. *J. Climate*, **9**, 840–858.
- Zhang, C., 1993: Large-scale variability of atmospheric deep convection in relation to sea surface temperature in the tropics. *J. Climate*, **6**, 1898–1913.
- Zhang, G. J., and N. A. McFarlane, 1995: Sensitivity of climate simulations to the parameterization of cumulus convection in the Canadian Climate Centre general circulation model. *Atmos.–Ocean*, **33**, 407–446.
- Zhou, T., B. Wu, and B. Wang, 2009: How well do atmospheric general circulation models capture the leading modes of the interannual variability of Asian–Australian monsoon? *J. Climate*, **22**, 1159–1173.